Photochemical Reduction of Oxygen Adsorbed to Nanocrystalline TiO_2 Films: A Transient Absorption and Oxygen Scavenging Study of Different TiO_2 Preparations

Ana M. Peiró,[†] Claudia Colombo,[†] Gerry Doyle,[‡] Jenny Nelson,[§] Andrew Mills,[‡] and James R. Durrant*[,†]

Departments of Chemistry and Physics, Imperial College London, Exhibition Road, London SW7 2AZ, United Kingdom, and Department of Pure and Applied Chemistry, University of Strathclyde, Glasgow, G1 1XL, United Kingdom

Received: July 20, 2006; In Final Form: September 6, 2006

Transient absorption spectroscopy (TAS) has been used to study the interfacial electron-transfer reaction between photogenerated electrons in nanocrystalline titanium dioxide (TiO_2) films and molecular oxygen. TiO_2 films from three different starting materials (TiO_2 anatase colloidal paste and commercial anatase/rutile powders Degussa TiO_2 P25 and VP TiO_2 P90) have been investigated in the presence of ethanol as a hole scavenger. Separate investigations on the photocatalytic oxygen consumption by the films have also been performed with an oxygen membrane polarographic detector. Results show that a correlation exists between the electron dynamics of oxygen consumption observed by TAS and the rate of oxygen consumption through the photocatalytic process. The highest activity and the fastest oxygen reduction dynamics were observed with films fabricated from anatase TiO_2 colloidal paste. The use of TAS as a tool for the prediction of the photocatalytic activities of the materials is discussed. TAS studies indicate that the rate of reduction of molecular oxygen is limited by interfacial electron-transfer kinetics rather than by the electron trapping/detrapping dynamics within the TiO_2 particles.

Introduction

TiO_2 has been extensively investigated for the photocatalytic purification of air and water. Upon band gap photoexcitation of TiO_2 (<350 nm), electron−hole pairs are generated in the material. If the appropriate electron acceptors (e.g., oxygen) and electron donors (e.g., organic molecules) are adsorbed onto the TiO_2 surface, interfacial electron-transfer reactions can result in the photocatalytic oxidation of the organic species. Oxygen is the usual electron acceptor employed in studies aimed at the use of semiconductor photocatalysis for environmental cleaning; its role in these reactions has been the focus of attention of several theoretical and experimental studies.[1−9] It is generally agreed that photogenerated electrons can reduce molecular oxygen to $O_2^{\bullet-}$,[10−12] which can subsequently transform to other chemical species, such as $HO_2^{\bullet}$, HO_2^-, H_2O_2, and possibly $OH^{\bullet}$ radicals.[3,7,13−15] These activated oxygen species may take part in the oxidation of the organic electron donor.[3,14−16] On the other hand, photogenerated holes can oxidize the electron donor (also referred to as the "hole scavenger"), either via the formation of reactive species such as surface-bound $OH^{\bullet}$ radicals or through direct reaction with adsorbed organic molecules.[1,17−19] Together, these reactions can ultimately result in the complete photomineralization of the organic compounds to carbon dioxide, water, and mineral acids.

In this study, we focus on the kinetics of the oxygen reduction component of the photocatalytic process in the presence of excess organic electron donors. Under these conditions, the reaction of these excess hole scavengers with photogenerated holes can compete efficiently with the electron−hole recombination reaction,[20,21] as we discuss in more detail below. These conditions result in the photogeneration of long-lived electrons, which achieve the reduction of oxygen and other species (Q) adsorbed onto the TiO_2 surface through the following reactions:

$$e^- + O_2 \rightarrow O_2^{\bullet-} \quad (1)$$

$$e^- + Q \rightarrow Q^{\bullet-} \quad (2)$$

where Q represents alternative electron acceptor species, including oxidized organics generated by the hole scavenging reaction. As such, kinetic competition between reactions 1 and 2 may determine the quantum yield for molecular oxygen reduction. In this paper, we focus on this kinetic competition as a function of oxygen concentration, employing three different TiO_2 film preparations.

Transient absorption spectroscopy (TAS) studies have shown that the induced absorption of photogenerated electrons and holes within the TiO_2 nanoparticles can be used to monitor the generation and decay dynamics of these species.[20,22−31] Femtosecond and picosecond transient absorption studies have revealed the time scales of the charge generation and trapping processes following photoexcitation.[23,32−36] Other studies at longer time scales have dealt with the interfacial electron-transfer reactions with adsorbed species. For example, spectroscopic evidence of the hole scavenging ability of reagents such as ethanol,[35] methanol,[17,19,20,35,37−39] 2-propanol,[17,35,40,41] dichloroacetate,[26] poly(vinyl alcohol),[18,24] *trans*-decalin,[42,43] iodide ions,[17] and thiocyanate[26,36,44] have been reported. On the other hand, time-resolved infrared[45,46] and visible[20] absorption spectroscopy studies have monitored the reaction of photogenerated

* Address correspondence to this author. E-mail: j.durrant@imperial.ac.uk. Fax: + (44) (0) 20 7594 5801.
[†] Department of Chemistry, Imperial College London.
[‡] University of Strathclyde.
[§] Departments of Physics, Imperial College London.

10.1021/jp064591c CCC: $33.50
Published on Web 10/20/2006

electrons in TiO_2 films with adsorbed oxygen, showing that the decay of the electron absorption within the TiO_2 catalyst is accelerated in the presence of oxygen. However, studies addressing the correlation between the observed electron decay kinetics and the overall photocatalytic activity have been very limited to date.[39,47,48]

The aim of the present study is to correlate directly the oxygen consumption observed during the photocatalytic process with the kinetics of electron transfer of photogenerated electrons within TiO_2 to molecular oxygen studied by TAS. The direct observation of oxygen consumption during the photocatalytic process has been the subject of relatively few studies,[9,20,21,49−52] most researchers focusing instead on the oxidative degradation of the organic compound to carbon dioxide and water. Recently, we have shown that it is possible to achieve the complete deoxygenation of a closed environment by UV-illumination of nanocrystalline TiO_2-based systems in the presence of excess organic electron donors.[20,21,52] Here, excess electron donors (referred to herein as "sacrificial" electron donors, SEDs) have been employed to allow us to focus on the oxygen dependence of the reaction mechanism. We consider the light-driven oxygen scavenging efficiency of TiO_2 films prepared from three different starting materials in the presence of ethanol as SED: a nanocrystalline TiO_2 colloidal paste (nc-TiO_2) prepared via an aqueous hydrolysis route and commercial anatase/rutile powders TiO_2 P25 and VP TiO_2 P90 (Degussa Ltd.) fabricated by flame pyrolysis. We monitor the extent of oxygen consumption in the photocatalytic process by means of an oxygen membrane polarographic detector, i.e., a Clark electrode, which allows films under test to be placed in an air-filled closed cell and the decrease of oxygen concentration to be monitored upon exposure to UV irradiation. Secondly, we employ transient absorption spectroscopy to monitor the dynamics of reactions 1 and 2 above. We correlate the electron dynamics observed by TAS for the different films with their rate of oxygen consumption through the photocatalytic process and discuss whether the observed oxygen reduction dynamics are limited by interfacial electron-transfer dynamics or by electron/oxygen transport dynamics to the interface.

Experimental Details

All chemicals used were obtained from Sigma-Aldrich or their subsidiaries, unless otherwise stated. TiO_2 powders (TiO_2 P25 and VP TiO_2 P90) were supplied by Degussa Ltd.

Sample Preparation. Fluorine-doped tin oxide conducting glass (15 Ω/square, Hertford Glass) was placed in acetone and sonicated for 30 min, then washed thoroughly with deionized water and dried in a furnace at 450 °C for 15 min. Titania particles from three different sources were assessed as photocatalysts, including nanocrystalline (nc)-TiO_2 synthesized by the aqueous hydrolysis of titanium isopropoxide and commercial TiO_2 powders TiO_2 P25 and VP TiO_2 P90. nc-TiO_2 colloids (∼15 nm) were prepared as described in previously published methods.[24,53,54] Mesoporous films (4 μm thickness) were deposited using the doctor-blade technique on the conducting glass substrates. The resulting films consisted of TiO_2 particles approximately 15 nm in diameter and over 90% anatase, as determined by Raman spectroscopy.[55] TiO_2 P25 is a nanoparticulate titania powder (typically 80:20 anatase/rutile, average anatase particle size 21 nm) widely recognized as the benchmark material for photocatalytic studies, while TiO_2 P90 is a new analogous preparation comprising smaller diameter nanoparticles of mainly anatase structure (>90% anatase, average anatase particle size 13 nm). Their surface areas were determined by Brunauer−Emmett−Teller (BET) analysis to be ∼100 $m^2\ g^{-1}$ for nc-TiO_2, 90 ± 20 $m^2\ g^{-1}$ for TiO_2 P90, and 50 ± 15 $m^2\ g^{-1}$ for TiO_2 P25. Films consisting of TiO_2 P25 and TiO_2 P90 particles were prepared from an ethanolic suspension of the powders. In a typical preparation, 1 g of TiO_2 was mixed with 8.5 or 4.5 mL of absolute ethanol, for TiO_2 P25 and TiO_2 P90, respectively. This suspension was sonicated for 30 min in a bath sonicator. Films were deposited by doctor-blading the paste following the same procedure as described for the preparation of nc-TiO_2 films.[53] Films were left to dry in an oven for 1 h at 70 °C prior to use. Selected samples were further calcined at 450 °C for 20 min. Films were stored under a dry atmosphere prior to measurement.

Characterization of Photocatalytic Activity. All measurements were conducted at room temperature. Oxygen concentration measurements were made with an oxygen membrane polarographic detector (Rank Brothers Ltd., Cambridge, UK). A drop of absolute ethanol was placed onto the TiO_2 film and the substrate was inserted in a home-built sample holder, as described in ref 21. UV-A 365 ± 25 nm fluorescent tubes (I = 6 mW cm^{-2}) were used as the irradiation source, resulting in a sample irradiance of 4.8 mW·cm^{-2}, similar to the intensity of UV-A solar irradiance. For transient absorption measurements, a PTI GL-3300 N_2-laser (337 nm, ∼400 μJ cm^{-2}, repetition rate 0.8 Hz) was used as the excitation source.[20] For measurements under different laser excitation intensities, optical transmission filters were placed between the nitrogen laser and the sample. TiO_2 films were inserted into a quartz cell that was provided with a plastic septum. A gas flow setup was arranged to measure the electron dynamics in the films as a function of oxygen/nitrogen and SED concentrations. Three different gas combinations were employed: (a) the quartz cell was purged with a premixed oxygen/nitrogen gas, the proportions of which were controlled by the use of flow meters; (b) a controlled oxygen/nitrogen flow was directed through a Dreschel bottle containing absolute ethanol before reaching the quartz cell—this configuration allowed work in an environment saturated with ethanol (58 300 ppm, 5.8%, of ethanol in gas phase)[56,57] in the presence of different oxygen concentrations; and (c) a single controlled nitrogen flow was directed through the Dreschel bottle containing absolute ethanol and, before reaching the quartz cell, the resulting flow was combined with the desired ratio of an additional controlled nitrogen flow. This last configuration provided the mechanism to work in an anaerobic environment in the presence of different ethanol concentrations. The gas was introduced into the quartz cell by means of a needle inserted in the septum and an additional needle was used to provide escape of the gas during the purge process. In all cases, the cell was purged for 1 h with the gas of desired characteristics and, after this period, both needles were removed, leaving the cell sealed and containing the desired concentrations of oxygen/nitrogen and ethanol.

Results

Oxygen Scavenging Ability of nc-TiO_2 Films. We considered first the ability of nc-TiO_2 films prepared from the colloidal TiO_2 paste to consume the molecular oxygen present in a sealed oxygen electrode cell. The experimental procedure involved the use of an oxygen electrode to monitor the gaseous oxygen concentration of the cell as a function of UV-A illumination time. Typical data are shown in Figure 1, in which complete deoxygenation of the cell air volume is achieved in less than 700 s when nc-TiO2 films are irradiated in the presence of ethanol as a SED. The oxygen consumption rates in Figure 1

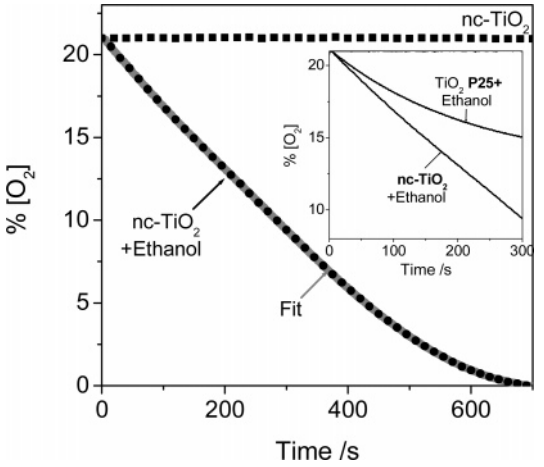

Figure 1. Oxygen consumption profiles (●) of nc-TiO_2 films in the presence of ethanol as a SED as a function of UV-A irradiation time in a closed cell. Control data for nc-TiO_2 films in the absence of ethanol are also shown (■). The gray line corresponds to a fit of the experimental oxygen scavenging data to the integrated Langmuir−Hinshelwood rate law, eq 3. The inset shows a comparison of the oxygen consumption profiles of nc-TiO_2 and TiO_2 P25 in the presence of ethanol as a SED.

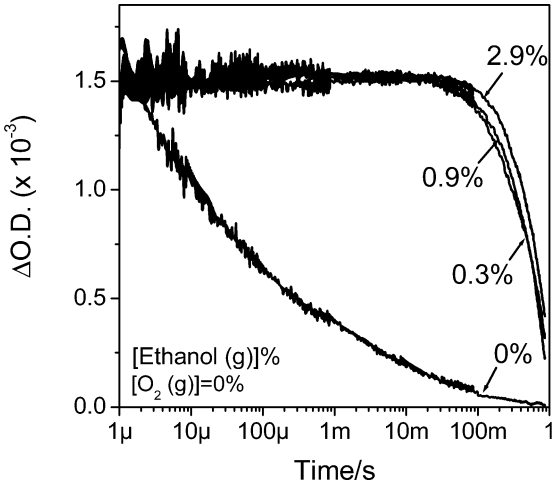

Figure 2. Transient absorption study of nc-TiO_2 films in anaerobic environment and in the presence of gas-phase ethanol in concentrations ranging from 0.3% to 2.9%. Data in the absence of ethanol (0%) are also shown. Data were collected at an excitation wavelength of 337 nm and a probe wavelength of 800 nm. ΔO.D. is the transient absorption change.

correspond to one oxygen molecule consumed for every ∼5 photons of UV-A light. Assuming that the overall process of oxygen consumption by TiO_2 photocatalysis requires four photogenerated electrons, as has been reported previously,[58,59] this suggests an absolute quantum efficiency for the process as high as ∼80%. This remarkably high quantum efficiency indicates that both the hole scavenging reaction and the reduction of molecular oxygen are occurring with near unity quantum efficiencies in these films. Control data in which nc-TiO_2 films were irradiated in the absence of ethanol showed negligible oxygen scavenging function. This fact highlights the efficiency of ethanol as a hole scavenger in the photocatalytic reaction,[29] which prevents the competing electron−hole recombination reaction, thus allowing the electrons to be available for the reduction of oxygen adsorbed onto the TiO_2 surface.

As shown in Figure 1, the rate of oxygen consumption of nc-TiO_2 films in the presence of ethanol is not strongly dependent upon oxygen concentration, resulting in efficient oxygen consumption even at low oxygen concentrations. Indeed, the kinetics of the oxygen consumption are zero order (i.e., show a linear decay of $[O_2(g)]$ with time) for high oxygen concentrations >5% (corresponding to an oxygen partial pressure of 0.05 atm), while approximately first order behavior (monoexponential decay) is observed for lower oxygen concentrations (<5%). As we have reported previously,[20] such behavior is in accordance with the Langmuir−Hinshelwood equation typically used to model the rate of photocatalytic destruction of organic pollutants by TiO_2. We fitted the experimental data to the integrated form of this equation as given by eq 3 (see ref 20 for details):

$$t = \frac{B[O_2]_0}{A}\left(1 - \frac{[O_2]}{[O_2]_0}\right) - \frac{1}{A}\ln\frac{[O_2]}{[O_2]_0} \qquad (3)$$

and a typical fit is shown in Figure 1 (gray line). Given that the equation includes only two variable parameters, *A* and *B*, the fit is in excellent agreement with the experimental data. The values of *A* and *B* determined from this fit are 0.022 s^{-1} and 1.25×10^4 M^{-1}, respectively (see the Supporting Information for a definition of these parameters).

Transient Absorption Studies of Oxygen Reduction with nc-TiO_2 Films. The electrochemical data presented above address the overall rate of light-driven oxygen consumption as a function of oxygen concentration. Through transient absorption studies, we are able to investigate directly the key step in the oxygen consumption process, the reduction of molecular oxygen by electrons photogenerated in the nc-TiO_2 films using ethanol as a SED. Our aim is to correlate the oxygen scavenging studies with the transient absorption data.

First, we evaluate spectroscopically the hole scavenging ability of ethanol in the absence of oxygen. Figure 2 shows typical transient absorption data obtained for nc-TiO_2 films in the presence of different concentrations of ethanol in the gas phase, under anaerobic conditions. The data were monitored at 800 nm, following low intensity band gap excitation of the nc-TiO_2 particles at 337 nm. In the absence of ethanol (Figure 2, 0%), the transient absorption signal exhibits a fast decay with a half-time, $t_{50\%}$, of ∼25 μs. According to previous studies,[20,21,32] this decay is assigned to the recombination of electrons and holes. The observed dynamics are highly dispersive, assigned, as we have discussed previously,[20] to the influence of charge trapping within an energetic distribution of trap depths. At higher excitation intensities, electron−hole recombination has been reported to take place on much faster time scales (less than 1 ns),[17] most probably due to trap filling resulting from the high excitation densities. In the presence of ethanol (Figure 2, concentrations ranging from 0.3% to 2.9% of ethanol in the gas phase), the rapid recombination phase is replaced by a long-lived ($t_{50\%} \approx 550$ ms) signal. The transient absortion spectrum of this long-lived signal exhibits a broad absorption increase in the red/near-infrared, with a maximum around 800 nm (see Figure S1 in the Supporting Information), confirming its assignment to photogenerated electrons in the TiO_2.[18,23,24,26,27,29−31] These observations indicate that ethanol acts as an efficient hole scavenger, consistent with previous spectroscopic studies,[24,35] and its reaction with photogenerated holes competes efficiently with the electron/hole recombination process even at concentrations as low as 0.3% ethanol. The observed long-lived decay in the absence of oxygen is assigned to the reduction of alternative electron acceptor species, eq 2 above. Possible candidates for these electron acceptors "Q" are oxidized species generated by the hole scavenging reaction or adventitious impurities. We observe the efficiency of this hole scavenging reaction to be independent of the presence of oxygen (the yield

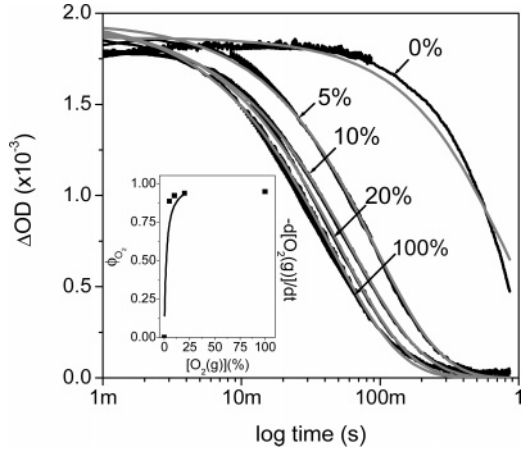

Figure 3. Transient absorption study of nc-TiO_2 films in an atmosphere saturated with ethanol in the gas phase (5.8%), under different oxygen concentrations ranging from 0% to 100%. Data were collected at an excitation wavelength of 337 nm and a probe wavelength of 800 nm. Black lines correspond to experimental data and gray lines are stretched exponential fits to the experimental data. The inset shows the yield of oxygen reduction (■) as a function of the oxygen concentration in the gas phase, calculated from TAS data with eq 4. The solid line in the inset corresponds to the rate of oxygen consumption determined from oxygen scavenging studies under continuous irradiance.

of the TAS signal assigned to long-lived electrons being independent of oxygen concentration, see below); the concentration of Q is therefore assumed to be oxygen independent. We note furthermore this slow decay is not expected to be due to the reduction of residual oxygen present in the system, as the transient decays are collected employing multiple laser pulses (>1000), during which any oxygen traces would be expected to be readily consumed.

As expected, when oxygen is incorporated into the system, the transient signal exhibits faster decays, assigned to electron reduction of molecular oxygen, eq 1 above. The transient absorption signal in the absence of ethanol (Figure 2, 0%), which exhibited a decay with a $t_{50\%}$ of ~25 μs under anaerobic conditions, decays with a $t_{50\%}$ of ~12 μs for an oxygen concentration of 21% (see Figure S2 in the Supporting Information), indicative of oxygen reduction competing directly with the electron/hole recombination reaction observed in the absence of hole scavengers. The observed half-time for the reduction of molecular oxygen by electrons is consistent with previous reports, where the characteristic time of this reaction was estimated at tens of microseconds.[20,26,45,46]

Further transient absorption studies were performed on nc-TiO_2 films under different oxygen concentrations in an ethanol-saturated environment, as shown in Figure 3. Even at oxygen concentrations as low as ~5%, the decay dynamics accelerate by almost an order of magnitude ($t_{50\%} \approx 70$ ms) relative to anaerobic conditions, assigned to rapid electron reduction of adsorbed molecular oxygen. Further increase in the oxygen concentration results in only a modest further acceleration of the dynamics ($t_{50\%}$ up to ~30 ms for [O_2(g)] = 100%). These dynamics exhibit approximately monoexponential decays; fits of the data to stretched exponential functions, $\Delta O.D. \propto \exp[-(t/\tau)^{\alpha}]$, where $\alpha = 1$ corresponds to a monoexponential decay, gave excellent fits with α in the range 0.83−1, as shown in Figure 3, with α decreasing with decreasing decay half-time. The dynamics were observed to be essentially independent of laser intensity in the range 40−400 μJ cm^{-2} pulse^{-1} and continuous UV-A background irradiance (4.8 mW cm^{-2}, comparable to solar irradiancies), as shown in the Supporting Information, indicating that these oxygen reduction dynamics are independent of the density of electrons in the TiO_2 film.

TABLE 1: Initial Rate of Oxygen Consumption, $r_i(O_2)$, of nc-TiO_2, TiO_2 P25, and TiO_2 P90 Films in Presence of Ethanol as a SED and UV-A Irradiation in a Closed Cell[a]

film composition	calcined at 450°C	$r_i(O_2)$ (s^{-1}) (±0.001)
nc-TiO_2	yes	−0.061
TiO_2 P90	yes	−0.046
TiO_2 P90	no	−0.042
TiO_2 P25	yes	−0.038
TiO_2 P25	no	−0.031

[a] Initial rate considered at 75 s of reaction. Films were studied as-prepared and after calcination at 450 °C for 20 min. Initial oxygen concentration is 21%.

The electron reduction of molecular oxygen monitored by the transient absorption data in Figure 3 is a bimolecular reaction, as specified by reaction 1. As such, it is striking that we observe essentially monoexponential and, therefore, first-order transient decays. This observation is indicative of the reaction being pseudo-first order, with one species being present in excess. Our observation that the reaction half-time is independent of laser excitation (and therefore electron density) indicates that it is the oxygen that is present in excess (i.e., the oxygen concentration accessible to TiO_2 electrons is not depleted significantly during the laser transients). The observation that the reaction half-time saturates at high oxygen concentrations is indicative of a saturation of available oxygen binding sites on the TiO_2 surface, and is consistent with the zeroth order oxygen scavenging data shown in Figure 1 over the same oxygen concentration range.

Comparison of Different Metal Oxides. We consider now the ability of two other TiO_2 preparations, namely Degussa P25 and P90 (see the Experimental Section for details), to consume the molecular oxygen present in a sealed oxygen electrode cell through the photocatalytic process. TiO_2 P25 and TiO_2 P90 powders are prepared in an industrial scale high-temperature flame reactor (T > 1000 °C),[60] while the nc-TiO_2 films are prepared by sol−gel techniques at much lower temperatures. The sol−gel films were calcined at 450 °C to eliminate the organics involved in the preparation and to sinter the colloidal particles, thus forming a nanocrystalline continuous network. For our studies on TiO_2 P25 and P90 films, we have used both noncalcined and calcined films to assess whether the sintering of the particles has an effect on the photocatalytic activity of the films. Table 1 shows the initial rate of oxygen consumption through the photocatalytic process for the three TiO_2 preparations under study, in the presence of ethanol as a SED, with an initial oxygen concentration of 21%. The ability of the films to scavenge oxygen in the presence of ethanol as a SED follows the order nc-TiO_2 > TiO_2 P90 > TiO_2 P25. Calcined films showed a slightly improved initial rate of oxygen consumption compared to noncalcined films. Furthermore, for both the TiO_2 P25 and the TiO_2 P90 films, the rate of oxygen consumption was observed to diminish as the oxygen concentration was lowered, as illustrated in the inset to Figure 1, with no observation of the zeroth order behavior reported for the nc-TiO_2 films over the oxygen concentration range studied.

Transient absorption studies were performed on nc-TiO_2, TiO_2 P25, and TiO_2 P90 films to investigate the electron dynamics underlying the different photocatalytic oxygen consumption rates of the three materials. Figure 4 shows a comparison of the TAS data obtained for the three TiO_2 preparations in an environment saturated with ethanol gas and in the presence of 20% oxygen. These conditions are equivalent to those at the initial stage of

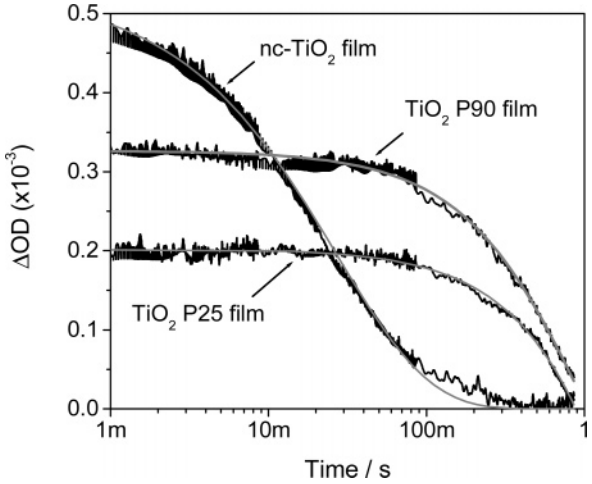

Figure 4. Transient absorption study of nc-TiO_2, noncalcined TiO_2 P90, and TiO_2 P25 films in an environment saturated with ethanol in the gas phase (5.8%) and oxygen concentration of 20%. Data were collected at an excitation wavelength of 337 nm and a probe wavelength of 800 nm. Solid gray lines correspond to stretched exponential decay fit to experimental data for nc-TiO_2 and monoexponential decay fits for data corresponding to TiO_2 P90 and TiO_2 P25 films.

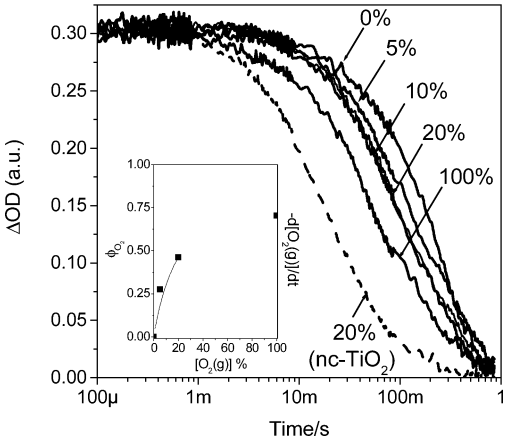

Figure 5. Transient absorption study of calcined TiO_2 P25 films in an atmosphere saturated with ethanol in the gas phase (5.8%), under different oxygen concentrations ranging from 0% to 100%. Data were collected at an excitation wavelength of 337 nm and a probe wavelength of 800 nm. The dashed line corresponds to nc-TiO_2 film in the presence of 20% oxygen, as reference data. As for Figure 3, the inset shows the yield of oxygen reduction (■) as a function of the oxygen concentration in the gas phase, with the solid line in the inset corresponding to the rate of oxygen consumption determined from oxygen scavenging studies.

the photocatalytic oxygen consumption studies summarized in Table 1. From this figure, it is evident that the initial optical density change for TiO_2 P90 and TiO_2 P25 films is lower than that for nc-TiO_2 films, while the electron lifetime is greatly increased in the former ($t_{50\%}$ values of 20, 370, and 450 ms for nc-TiO_2, TiO_2 P90, and TiO_2 P25 films, respectively). The lower initial amplitudes of the transient signals for the P25 and P90 films are indicative of lower yields of long-lived electrons, while the slower decay dynamics observed for these films are indicative of slower electron reduction of molecular oxygen. As for Figure 3, these transients all exhibited near monoexponential behavior (values of $\alpha = 0.86$, 1.0, and 1.0 from fits to stretched exponentials for nc-TiO_2, TiO_2 P90, and TiO_2 P25 films, respectively).

Further consideration of the kinetics of electron reduction of molecular oxygen was undertaken by TAS studies of calcined and uncalcined TiO_2 P25 and TiO_2 P90 films under different oxygen concentrations, in an ethanol saturated environment. Figure 5 shows the corresponding TAS data obtained for calcined TiO_2 P25 films. As observed previously for nc-TiO_2 films, the electron decay dynamics accelerate as the concentration of oxygen in the cell increases, assigned to increasingly rapid electron reduction of molecular oxygen, as discussed previously. It is apparent that this acceleration shows a smaller dependence on the oxygen concentration than that observed for nc-TiO_2 films (Figure 3), and does not saturate over the oxygen concentration range studied (up to 100%). Observations with uncalcined TiO_2 P25 films and TiO_2 P90 films (not shown) were qualitatively similar to those shown in Figure 5. The correlation between these transient absorption data and the oxygen scavenging efficiency will be discussed in detail below.

Discussion

We have experimentally studied the photochemical reduction of oxygen adsorbed to nanocrystalline TiO_2 films by two methods: (1) an oxygen membrane polarographic detector has allowed to directly monitor the photocatalytic oxygen consumption by the films in the presence of a hole scavenger and (2) transient absorption spectroscopy (TAS) studies have been used to investigate the interfacial electron-transfer reaction between photogenerated electrons in the TiO_2 films and molecular oxygen. Three different TiO_2 preparations have been investigated, namely nc-TiO_2, TiO_2 P25, and TiO_2 P90. The ability of the films to scavenge oxygen in the presence of ethanol as a SED follows the order nc-TiO_2 > TiO_2 P90 > TiO_2 P25. Other studies in the literature have also reported pure anatase powders with higher photocatalytic efficiency than TiO_2 P25 in the gas phase[61,62] and the higher photocatalytic activity of TiO_2 P90 compared to TiO_2 P25 is consistent with the higher surface area of the former, favoring surface-electron-transfer reactions over bulk electron−hole recombination.[21] However, we find that a strict comparison with other works is difficult, as the usually reported experimental conditions differ from the ones of the present study, such as working in aqueous media, with little hole scavenger and an excess of oxygen, contrary to our experimental conditions in the gas phase, where an excess of hole scavenger and low concentrations of oxygen are employed.

Qualitatively, we have observed clear correlations between the photocatalytic oxygen consumption data and the electron dynamics of oxygen reduction studied by TAS. The highest consumption and fastest oxygen reduction dynamics were observed for films fabricated from nc-TiO_2 colloidal paste. For these films, the rate of oxygen consumption was observed to be zeroth order in oxygen concentration for $[O_2(g)] > \sim 5\%$, consistent with our observation that kinetics of electron reduction of molecular oxygen also become oxygen concentration independent for $[O_2(g)] > \sim 5\%$. For TiO_2 P25 and TiO_2 P90 films, no zeroth order (oxygen concentration independent) oxygen consumption behavior was observed, correlating with the kinetics of electron reduction of oxygen being oxygen concentration dependent at all oxygen concentrations studied. We now consider in more detail the electron-transfer kinetics resolved in the transient absorption process, and their relationship to the efficiency of the photocatalytic process.

The oxygen reduction dynamics observed in the TAS data shown above result from two sequential processes: electron transport within the TiO_2 nanoparticles to surface sites and subsequent interfacial electron transfer to molecular oxygen. It is striking that these dynamics are remarkably slower and less dispersive than those observed in analogous studies of charge recombination to sensitizer dye cations.[63,64] We have previously

shown that the interfacial charge transfer rate constant depends strongly on the spatial separation of the electron accepting orbital (the dye cation HOMO orbital) from the TiO_2 surface.[65−68] In those studies, a shift from faster and more dispersive electron dynamics to slower and near monoexponential behavior was observed when the spatial separation of the HOMO orbital from the TiO_2 surface was increased. The latter behavior is indicative of the charge recombination being limited by the interfacial electron dynamics rather than by the electron transport within the TiO_2 nanoparticles. The correlation between recombination half-time and the dispersive nature of the dynamics is again observed for the oxygen reduction dynamics reported herein, with the faster dynamics observed at high oxygen concentrations with nc-TiO_2 films showing significant deviations from monoexponential behavior ($\alpha \approx 0.8$). However, it is striking that, given the small size of an O_2 molecule compared to a molecular sensitizer, the oxygen reduction dynamics we report here are remarkably slow, orders of magnitude slower than those we would expect for recombination to a molecular sensitizer of comparable size. One possible limitation could be the presence of only a few sites on the TiO_2 nanoparticle surface suitable for the charge transfer. However, quantitative comparison with the dynamics observed for dye sensitized films suggests that the density of suitable sites would need to be $\ll 1$ per nanoparticle, a conclusion difficult to reconcile with reports of efficient photocatalytic reactions by titania powders where photogenerated electrons and holes would be confined to a single nanoparticle (or small number of nanoparticles). Alternatively, a slow interfacial electron-transfer rate constant could derive from a low energetic driving force resulting in a large activation energy for the reaction.[4,7,51,52] A low driving force would be consistent with the small difference between estimates of the TiO_2 conduction band edge (−0.6 V vs NHE, at pH 7)[18] relative to the O_2/O_2^- reduction potential (−0.33 V vs NHE).[69,70] (The values of redox potentials derived from homogeneous studies are used with the assumption that they are the best possible approximation of the interfacial situation.[26]) This low driving force would be further reduced if the electron transfer takes place from surface electron traps (for anatase nc-TiO_2 and TiO_2 P25 films, trap states at about 0.5−0.7 eV[71,72] and 0.5−0.6 eV[73] below the conduction band edge have been reported, respectively; and for rutile, trap states have been detected at depth levels ranging from 0.21 to 0.87 eV below its conduction band edge[74]). Finally we note that comparison of transient absorption data collected in the presence (Figure 3) and absence (Figure S2 of the Supporting Information) of ethanol suggests that the presence of ethanol may itself significantly retard the kinetics of electron reduction of molecular oxygen. The contribution of transient absorption from photogenerated holes to the data shown in Figure S2 does complicate analysis of these data. Nevertheless, this observation raises the possibility that the adsorption of organics, such as ethanol, to the surface of the TiO_2 may function as a physical barrier layer impeding electron reduction of molecular oxygen either by increasing the spatial separation of molecular oxygen from the film surface or by passivating oxygen binding sites.

Slow interfacial electron-transfer kinetics of oxygen reduction by TiO_2 electrons may limit the efficiency of the overall photocatalytic reaction in two ways. Studies by Gerischer et al.[1,2,75,76] have suggested that the overall rate of photocatalytic degradation can be limited by a slow rate of electron transfer from the TiO_2 particles to oxygen. Under these conditions, an excess of electrons would accumulate on the TiO_2 particles until the overall rates of electron and hole charge transfer become matched. As a consequence of the increased electron density, the rate of electron−hole recombination would increase, resulting in a reduction in the overall efficiency of the photocatalytic process.[8] However, our observation that the electron decay dynamics are independent of continuous background irradiance, conditions expected to result in maximal background electron density in the film, indicates that electron accumulation in the film is not a significant factor. This conclusion is consistent with simple estimates of the expected extent of electron accumulation in the film under continuous UV irradiation using the electron lifetime observed in the presence of >5% oxygen (<70 ms), which would indicate that continuous solar irradiation would result in accumulation of only approximately one electron per nanoparticle. This calculation supports our conclusion that enhanced recombination losses resulting from electron accumulation are unlikely to be a significant factor determining photocatalytic efficiency for the films studied here.

The alternative mechanism whereby oxygen reduction may limit the efficiency of the photocatalytic reaction is by kinetic competition between the two reactions detailed in eqs 1 and 2 above. As such, the quantum yield of oxygen reduction can be defined as:

$$\phi_{O_2^-} = \frac{k_1'}{k_1' + k_2'} = 1 - \frac{t_{50\%}}{t_{50\%}^{\ 0}} \qquad (4)$$

where k_1' and k_2' are the pseudo-first-order effective rate constants for reactions 1 and 2, respectively, and $t_{50\%}$ and $t_{50\%}^{\ 0}$ are the electron decay half-times in the presence and absence of oxygen, respectively. Insets in Figures 3 and 5 show plots of oxygen concentration versus $\phi_{O_2^-}$ (determined via eq 4 from the transient absorption data) and the rate of oxygen consumption ($-d[O_2(g)]/dt$, determined from the electrochemical data) for nc-TiO_2 and TiO_2 P25 films, respectively. It is apparent that a reasonable agreement is obtained between the oxygen reduction yields measured by the TAS studies and rates of oxygen consumption measured by the oxygen electrode, strongly indicating that kinetic competition between reactions 1 and 2 may be a significant factor limiting the efficiency of oxygen reduction, and thereby the overall photocatalytic process.

Our observation that, for the nc-TiO_2 films, the overall rate of the photocatalytic reaction becomes oxygen independent for high oxygen concentrations is consistent with previous literature studies. For example, Kormann et al.[77] have reported that under air-saturation conditions, the rate of trichloromethane degradation was essentially independent of the oxygen concentration. Bideau and co-workers reported that the rate of oxidation of acetic acid in water by TiO_2 became independent of the oxygen concentration for concentrations over 3 ppm[78] (for reference, oxygen concentration in air-saturated water is ∼8 ppm). Our transient absorption studies reported here clearly indicate that this oxygen concentration independence results from saturation of the available oxygen binding sites on the TiO_2 surface, resulting in saturation of the kinetics of reduction of molecular oxygen by photogenerated electrons. It is striking, however, that this saturation behavior is not observed for the P25 and P90 films. For these films, the rate of oxygen consumption (monitored electrochemically) is oxygen concentration dependent up to 21% oxygen (the highest oxygen concentrations studied), consistent with the half time of oxygen reduction monitored by the TAS studies also shortening continuously as the oxygen concentration is increased. This behavior can be most easily rationalized in a lower oxygen binding constant for the TiO_2 P25 and TiO_2 P90 films, such that even at 21% oxygen, these binding sites are not fully occupied.

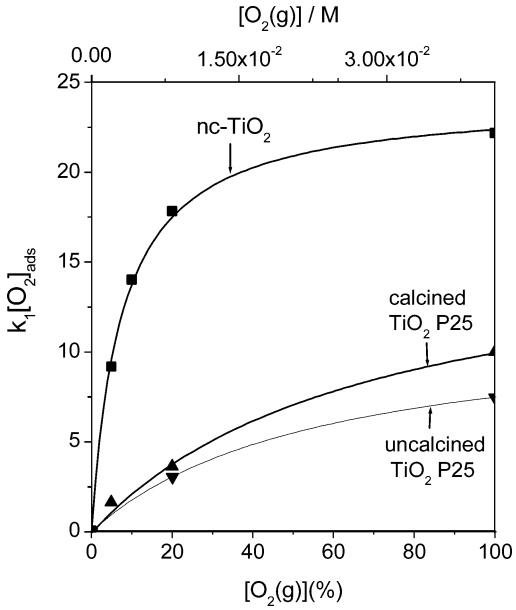

Figure 6. Relative concentration of oxygen molecules adsorbed onto nc-TiO_2 (■), calcined TiO_2 P25 (▲), and uncalcined TiO_2 P25 (▼) films as a function of the concentration of oxygen in the bulk phase (ranging from 0% to 100%) in an atmosphere saturated with ethanol in the gas phase (5.8%) determined from the transient absorption data. Solid lines correspond to the fit of the experimental data to the Langmuir adsorption isotherm, eq 6.

Quantification of the oxygen binding constants for the three different films can be obtained from a Langmuir Adsorption Isotherm analysis of the transient absorption data. The pseudo-first-order rate constant for reaction 1, k_1', is given by

$$k_1' = k_1[O_2]_{ads} \tag{5}$$

where k_1 is the second-order rate constant for the reaction and $[O_2]_{ads}$ is the concentration of adsorbed oxygen molecules on the TiO_2 surface. As k_1' can be determined directly from the decay times of the absorption transients ($k_1' = \ln 2/t_{50\%}$), this allows us to plot the relative concentration of adsorbed oxygen as a function of the bulk oxygen concentration, as shown in Figure 6 for three different TiO_2 films. These data were fitted to the standard Langmuir adsorption isotherm

$$[O_2]_{ads} = \frac{K_{O_2}[O_2(g)][O_2]^{bs}}{1 + K_{O_2}[O_2(g)]} \tag{6}$$

where K_{O_2} is the equilibrium adsorption constant for oxygen binding, and $[O_2]^{bs}$ is the concentration of oxygen binding sites. We obtain K_{O_2} values of 330, 36, and 43 M^{-1} for nc-TiO_2, calcined TiO_2 P25, and uncalcined TiO_2 P25 films, respectively. Similar values were obtained for TiO_2 P90 films as for TiO_2 P25. The equilibrium adsorption constants of oxygen we report here are of the same order as those reported by Addamo et al.[79] in the gas−solid regime for a TiO_2 catalyst (Merck) and for TiO_2 Degussa P25 (240 and 90 M^{-1}, respectively). The lower equilibrium adsorption constants for TiO_2 P25 and TiO_2 P90 films compared to nc-TiO_2 are consistent with the stronger dependence upon bulk oxygen concentration of both the oxygen scavenging rates determined by the oxygen electrode and the electron decay times observed in the TAS studies. In contrast, the higher oxygen adsorption constant determined for the nc-TiO_2 results in saturation of the oxygen binding sites for bulk oxygen concentrations ($[O_2(g)]$) > 5%, as evidenced by both the oxygen scavenging rates and electron decay times being independent of $[O_2(g)]$ for $[O_2(g)]$ > 5%.

Extrapolation of the fits of the Langmuir adsorption isotherms shown in Figure 6 to saturating oxygen concentration give estimates for the saturating pseudo-first-order rate constants, $k_1' = k_1[O_2]^{bs}$, when all oxygen binding sites are occupied. While this extrapolation clearly has significant errors, it is apparent that this effective rate constant is significantly higher for nc-TiO_2 compared to the TiO_2 P25 and P90 films. This observation would be consistent with lower density of oxygen binding sites $[O_2]^{bs}$ on the TiO_2 P25 and P90 films relative to nc-TiO_2. Alternatively, this observation could also result from differences in the interfacial electron-transfer rate constant k_1, due perhaps to the P25 and P90 oxygen binding sites being physically less accessible to electrons in those materials or the activation barrier for oxygen reduction being higher. Different surface morphologies (e.g., hydroxylation density or ethanol adsorption coverage) may also be expected to affect the interfacial charge-transfer rate constant.

Finally, we note that the different oxygen scavenging rates observed for the three films may also result from different yields of long-lived electrons. Figure 4 indicates that the amplitude of the initial ΔO.D. signal assigned to long-lived electrons is in the order nc-TiO_2 > TiO_2 P90 > TiO_2 P25 films, paralleling the trend in oxygen scavenging efficiencies. It is possible that this trend in ΔO.D. signal amplitude may simply result from differences in the molar absorption coefficient (ϵ) of the electrons in the TiO_2 films. Alternatively, this trend could result from differing scattering properties of the films, the nc-TiO_2 films being the least scattering and the TiO_2 P25 films being the most. Finally, we note this trend could also result from different efficiencies of the hole scavenging reaction, resulting in more signficant submicrosecond charge recombination losses for the TiO_2 P90 and P25 films. Such differences could arise from different densities of defects/trap sites for the TiO_2 preparations resulting from their dissimilar surface and processing temperatures. It has been reported that the high-temperature flame process is expected to yield fewer defect sites on the TiO_2 P25 particles, compared to sol−gel TiO_2 particles.[42]

Conclusions

We have experimentally studied the photochemical reduction of oxygen adsorbed to nanocrystalline TiO_2 films by two methods: (1) an oxygen membrane polarographic detector has allowed to directly monitor the photocatalytic oxygen consumption by the films in the presence of a hole scavenger and (2) transient absorption spectroscopy (TAS) studies have been used to investigate the interfacial electron-transfer reaction between photogenerated electrons in the TiO_2 films and molecular oxygen. Three different TiO_2 preparations have been investigated, namely, nc-TiO_2, TiO_2 P25, and TiO_2 P90. The ability of the films to scavenge oxygen in the presence of ethanol as a SED follows the order nc-TiO_2 > TiO_2 P90 > TiO_2 P25. A correlation was found between the photocatalytic oxygen consumption and the electron dynamics of oxygen scavenging studied by TAS in the presence of different concentrations of oxygen and ethanol in the gas phase. The fastest scavenging and fastest oxygen reduction dynamics were observed for films fabricated from nc-TiO_2 colloidal paste. For this film, both the rate of oxygen scavenging and the kinetics of oxygen reduction were observed to be independent of oxygen concentration for $[O_2(g)]$ > 5%. For the TiO_2 P25 and P90 films, the electron reduction dynamics were an order of magnitude slower and oxygen concentration dependent for all concentrations studied,

correlating with less efficient, and oxygen concentration dependent, oxygen scavenging. Through the analysis of the decay functions in relation with the oxygen consumption studies, we have reached the conclusion that the rate of interfacial electron transfer between the photogenerated electrons in the three TiO_2 films and molecular oxygen in the surrounding atmosphere is slow, and therefore this is the limiting step in the reaction kinetics. This process has been found to be slower for TiO_2 P25 and TiO_2 P90 than for nc-TiO_2. Several hypotheses have been discussed that could account for the experimental observations.

Acknowledgment. We thank Degussa Ltd. for providing TiO_2 P25 and VP TiO_2 P90 photocatalysts and the EPSRC for financial support. Ana M. Peiró acknowledges the Spanish Secretaría de Estado de Universidades e Investigación del Ministerio de Educación y Ciencia for a Postdoctoral fellowship. We also thank the reviewers for helpful comments on the effect of ethanol adsorption.

Supporting Information Available: Details of the kinetic model of oxygen consumption; plots of the transient absorption signal of nc-TiO_2 film in the presence of ethanol gas in aerobic environment, the transient absorption signal of nc-TiO_2 film in the absence of ethanol in the gas phase under anaerobic and aerobic conditions, exitation intensity dependence of the transient absorption signal for nc-TiO_2 films in an ethanol gas-saturated environment under anaerobic and aerobic environments, and the transient absorption signal of nc-TiO_2 film in an ethanol gas-saturated environment and aerobic conditons in the absence and presence of continuous UV-A bias light irradiation; a listing of the half-lives for each excitation intensity obrtained from the TAS for nc-TiO_2 films. This material is available free of charge via the Internet at http://pubs.acs.org.

References and Notes

(1) Gerischer, H.; Heller, A. *J. Phys. Chem.* **1991**, *95*, 5261−5267.
(2) Gerischer, H.; Heller, A. *J. Electrochem. Soc.* **1992**, *139*, 113−118.
(3) Schwitzgebel, J.; Ekerdt, J. G.; Gerischer, H.; Heller, A. *J. Phys. Chem.* **1995**, *99*, 5633−5638.
(4) Kesselman, J. M.; Shreve, G. A.; Hoffmann, M. R.; Lewis, N. S. *J. Phys. Chem.* **1994**, *98*, 13385−13395.
(5) Upadhya, S.; Ollis, D. F. *J. Phys. Chem. B* **1997**, *101*, 2625−2631.
(6) Sukharev, V.; Kershaw, R. *J. Photochem. Photobiol., A* **1996**, *98*, 165−169.
(7) Ahmed, S.; Fonseca, S. M.; Kemp, T. J.; Unwin, P. R. *J. Phys. Chem. B* **2003**, *107*, 5892−5900.
(8) Wang, C. M.; Heller, A.; Gerischer, H. *J. Am. Chem. Soc.* **1992**, *114*, 5230−5234.
(9) Fonseca, S. M.; Barker, A. L.; Ahmed, S.; Kemp, T. J.; Unwin, P. R. *Chem. Commun.* **2003**, 1002−1003.
(10) Remillard, J. T.; McBride, J. R.; Nietering, K. E.; Drews, A. R.; Zhang, X. *J. Phys. Chem. B* **2000**, *104*, 4440−4447.
(11) Ishibashi, K.; Fujishima, A.; Watanabe, T.; Hashimoto, K. *J. Phys. Chem. B* **2000**, *104*, 4934−4938.
(12) Berger, T.; Sterrer, M.; Diwald, O.; Knozinger, E.; Panayotov, D.; Thompson, T. L.; Yates, J. T. *J. Phys. Chem. B* **2005**, *109*, 6061−6068.
(13) Linsebigler, A. L.; Lu, G. Q.; Yates, J. T. *Chem. Rev.* **1995**, *95*, 735−758.
(14) Henderson, M. A.; Epling, W. S.; Perkins, C. L.; Peden, C. H. F.; Diebold, U. *J. Phys. Chem. B* **1999**, *103*, 5328−5337.
(15) Nakamura, R.; Imanishi, A.; Murakoshi, K.; Nakato, Y. *J. Am. Chem. Soc.* **2003**, *125*, 7443−7450.
(16) Vinodgopal, K.; Stafford, U.; Gray, K. A.; Kamat, P. V. *J. Phys. Chem.* **1994**, *98*, 6797−6803.
(17) Rabani, J.; Yamashita, K.; Ushida, K.; Stark, J.; Kira, A. *J. Phys. Chem. B* **1998**, *102*, 1689−1695.
(18) Micic, O. I.; Zhang, Y. N.; Cromack, K. R.; Trifunac, A. D.; Thurnauer, M. C. *J. Phys. Chem.* **1993**, *97*, 7277−7283.
(19) Micic, O. I.; Zhang, Y. N.; Cromack, K. R.; Trifunac, A. D.; Thurnauer, M. C. *J. Phys. Chem.* **1993**, *97*, 13284−13288.
(20) Xiao-e, L.; Green, A. N. M.; Haque, S. A.; Mills, A.; Durrant, J. R. *J. Photochem. Photobiol., A* **2004**, *162*, 253−259.
(21) Peiro, A. M.; Doyle, G.; Mills, A.; Durrant, J. R. *Adv. Mater.* (*Weinheim, Ger.*) **2005**, *17*, 2365−2368.
(22) Tachikawa, T.; Tojo, S.; Fujitsuka, M.; Majima, T. *Langmuir* **2004**, *20*, 9441−9444.
(23) Serpone, N.; Lawless, D.; Khairutdinov, R.; Pelizzetti, E. *J. Phys. Chem.* **1995**, *99*, 16655−16661.
(24) Bahnemann, D.; Henglein, A.; Lilie, J.; Spanhel, L. *J. Phys. Chem.* **1984**, *88*, 709−711.
(25) Bahnemann, D.; Henglein, A.; Spanhel, L. *Faraday Discuss.* **1984**, 151−163.
(26) Bahnemann, D. W.; Hilgendorff, M.; Memming, R. *J. Phys. Chem. B* **1997**, *101*, 4265−4275.
(27) Yoshihara, T.; Katoh, R.; Furube, A.; Tamaki, Y.; Murai, M.; Hara, K.; Murata, S.; Arakawa, H.; Tachiya, M. *J. Phys. Chem. B* **2004**, *108*, 3817−3823.
(28) Vinodgopal, K.; Bedja, I.; Hotchandani, S.; Kamat, P. V. *Langmuir* **1994**, *10*, 1767−1771.
(29) Jakob, M.; Levanon, H.; Kamat, P. V. *Nano Lett.* **2003**, *3*, 353−358.
(30) Kamat, P. V.; Bedja, I.; Hotchandani, S. *J. Phys. Chem.* **1994**, *98*, 9137−9142.
(31) Kolle, U.; Moser, J.; Gratzel, M. *Inorg. Chem.* **1985**, *24*, 2253−2258.
(32) Rothenberger, G.; Moser, J.; Gratzel, M.; Serpone, N.; Sharma, D. K. *J. Am. Chem. Soc.* **1985**, *107*, 8054−8059.
(33) Skinner, D. E.; Colombo, D. P.; Cavaleri, J. J.; Bowman, R. M. *J. Phys. Chem.* **1995**, *99*, 7853−7856.
(34) Furube, A.; Asahi, T.; Masuhara, H.; Yamashita, H.; Anpo, M. *J. Phys. Chem. B* **1999**, *103*, 3120−3127.
(35) Tamaki, Y.; Furube, A.; Murai, M.; Hara, K.; Katoh, R.; Tachiya, M. *J. Am. Chem. Soc.* **2006**, *128*, 416−417.
(36) Colombo, D. P.; Bowman, R. M. *J. Phys. Chem.* **1996**, *100*, 18445−18449.
(37) Yamakata, A.; Ishibashi, T. A.; Onishi, H. *J. Photochem. Photobiol., A* **2003**, *160*, 33−36.
(38) Yamakata, A.; Ishibashi, T.; Onishi, H. *J. Phys. Chem. B* **2002**, *106*, 9122−9125.
(39) Yamakata, A.; Ishibashi, T. A.; Onishi, J. *J. Phys. Chem. B* **2003**, *107*, 9820−9823.
(40) Yamakata, A.; Ishibashi, T.; Onishi, H. *Chem. Phys. Lett.* **2003**, *376*, 576−580.
(41) Schindler, K. M.; Kunst, M. *J. Phys. Chem.* **1990**, *94*, 8222−8226.
(42) Martin, S. T.; Herrmann, H.; Choi, W. Y.; Hoffmann, M. R. *J. Chem. Soc., Faraday Trans.* **1994**, *90*, 3315−3322.
(43) Martin, S. T.; Herrmann, H.; Hoffmann, M. R. *J. Chem. Soc., Faraday Trans.* **1994**, *90*, 3323−3330.
(44) Lawless, D.; Serpone, N.; Meisel, D. *J. Phys. Chem.* **1991**, *95*, 5166−5170.
(45) Yamakata, A.; Ishibashi, T.; Onishi, H. *J. Mol. Catal. A*: *Chem.* **2003**, *199*, 85−94.
(46) Yamakata, A.; Ishibashi, T.; Onishi, H. *J. Phys. Chem. B* **2001**, *105*, 7258−7262.
(47) Takeshita, K.; Yamashita, A.; Ishibashi, T.; Onishi, H.; Nishijima, K.; Ohno, T. *J. Photochem. Photobiol., A* **2006**, *177*, 269−275.
(48) Tachikawa, T.; Tojo, S.; Fujitsuka, M.; Majima, T. *Tetrahedron Lett.* **2004**, *45*, 3753−3756.
(49) Kim, Y. C.; Lee, K. H.; Sasaki, S.; Hashimoto, K.; Ikebukuro, K.; Karube, I. *Anal. Chem.* **2000**, *72*, 3379−3382.
(50) Kim, Y. C.; Sasaki, S.; Yano, K.; Ikebukuro, K.; Hashimoto, K.; Karube, I. *Anal. Chem.* **2002**, *74*, 3858−3864.
(51) Lee, K. H.; Kim, Y. C.; Suzuki, H.; Ikebukuro, K.; Hashimoto, K.; Karube, I. *Electroanalysis* **2000**, *12*, 1334−1338.
(52) Mills, A.; Doyle, G.; Peiro, A. M.; Durrant, J. *J. Photochem. Photobiol., A* **2006**, *177*, 328−331.
(53) Willis, R. L.; Olson, C.; O'Regan, B.; Lutz, T.; Nelson, J.; Durrant, J. R. *J. Phys. Chem. B* **2002**, *106*, 7605−7613.
(54) Barbe, C. J.; Arendse, F.; Comte, P.; Jirousek, M.; Lenzmann, F.; Shklover, V.; Gratzel, M. *J. Am. Ceram. Soc.* **1997**, *80*, 3157−3171.
(55) Green, A. N. M.; Chandler, R. E.; Haque, S. A.; Nelson, J.; Durrant, J. R. *J. Phys. Chem. B* **2005**, *109*, 142−150.
(56) Garriga, R.; Martinez, S.; Perez, P.; Gracia, M. *Fluid Phase Equilib.* **2003**, *207*, 97−109.
(57) Canadian Centre for Occupational Health & Safety, CCOHS, 2006.
(58) Kormann, C.; Bahnemann, D. W.; Hoffmann, M. R. *Environ. Sci. Technol.* **1988**, *22*, 798−806.
(59) Parkinson, B.; Decker, F.; Juliao, J. F.; Abramovich, M.; Chagas, H. C. *Electrochim. Acta* **1980**, *25*, 521−525.
(60) Degussa *Technical Information*; 05.
(61) Martra, G. *Appl. Catal., A*: *Gen.* **2000**, *200*, 275−285.

(62) Augugliaro, V.; Coluccia, S.; Garcia-Lopez, E.; Loddo, V.; Marci, G.; Martra, G.; Palmisano, L.; Schiavello, M. *Top. Catal.* **2005**, *35*, 237−244.

(63) Haque, S. A.; Tachibana, Y.; Willis, R. L.; Moser, J. E.; Gratzel, M.; Klug, D. R.; Durrant, J. R. *J. Phys. Chem. B* **2000**, *104*, 538−547.

(64) Tachibana, Y.; Haque, S. A.; Mercer, I. P.; Durrant, J. R.; Klug, D. R. *J. Phys. Chem. B* **2000**, *104*, 1198−1205.

(65) Clifford, J. N.; Palomares, E.; Nazeeruddin, M. K.; Gratzel, M.; Nelson, J.; Li, X.; Long, N. J.; Durrant, J. R. *J. Am. Chem. Soc.* **2004**, *126*, 5225−5233.

(66) Haque, S. A.; Handa, S.; Peter, K.; Palomares, E.; Thelakkat, M.; Durrant, J. R. *Angew. Chem., Int. Ed.* **2005**, *44*, 5740−5744.

(67) Hirata, N.; Lagref, J. J.; Palomares, E. J.; Durrant, J. R.; Nazeeruddin, M. K.; Gratzel, M.; Di Censo, D. *Chem. Eur. J.* **2004**, *10*, 595−602.

(68) Clifford, J. N.; Yahioglu, G.; Milgrom, L. R.; Durrant, J. R. *Chem. Commun.* **2002**, 1260−1261.

(69) Bielski, B. H. J.; Cabelli, D. E.; Arudi, R. L.; Ross, A. B. *J. Phys. Chem. Ref. Data* **1985**, *14*, 1041−1100.

(70) Wood, P. M. *FEBS Lett.* **1974**, *44*, 22−24.

(71) Boschloo, G.; Fitzmaurice, D. *J. Phys. Chem. B* **1999**, *103*, 2228−2231.

(72) Redmond, G.; Fitzmaurice, D.; Graetzel, M. *J. Phys. Chem.* **1993**, *97*, 6951−6954.

(73) Boschloo, G. K.; Goossens, A. *J. Phys. Chem.* **1996**, *100*, 19489−19494.

(74) Ghosh, A. K.; Wakim, F. G.; Addiss, R. R., Jr. *Phys. Rev.* **1969**, *184*, 979−988.

(75) Gerischer, H. *Electrochim. Acta* **1993**, *38*, 3−9.

(76) Gerischer, H. *J. Phys. Chem.* **1991**, *95*, 1356−1359.

(77) Kormann, C.; Bahnemann, D. W.; Hoffmann, M. R. *Environ. Sci. Technol.* **1991**, *25*, 494−500.

(78) Bideau, M.; Claudel, B.; Faure, L.; Kazouan, H. *J. Photochem. Photobiol., A* **1991**, *61*, 269−280.

(79) Addamo, M.; Augugliaro, V.; Coluccia, S.; Faga, M. G.; Garcia-Lopez, E.; Loddo, V.; Marci, G.; Martra, G.; Palmisano, L. *J. Catal.* **2005**, *235*, 209−220.